Electronic structure study of LaCoIn_{5} and its comparison with CeCoIn_{5}

Q. Y. Chen, X. B. Luo, E. Vescovo, K. Kaznatcheev, F. J. Walker, C. H. Ahn, Z. F. Ding, Z. H. Zhu, L. Shu, Y. B. Huang, and J. Jiang

Phys. Rev. B **100**, 035117 — Published 17 July 2019

DOI: 10.1103/PhysRevB.100.035117

Electronic structure study of $LaCoIn_5$ and its comparison with $CeCoIn_5$

Q. Y. Chen,[1,*] X. B. Luo,[1] E. Vescovo,[2] K. Kaznatcheev,[2] F. J. Walker,[3] C. H. Ahn,[3] Z. F. Ding,[4] Z. H. Zhu,[4] L. Shu,[4] Y. B. Huang,[5] and J. Jiang[3,†]

[1]*Science and Technology on Surface Physics and Chemistry Laboratory, Mianyang 621908, China*
[2]*National Synchrotron Light Source II, Brookhaven National Laboratory, Upton, New York 11973, USA*
[3]*Department of Applied Physics, Yale University, New Haven, Connecticut 06511, USA*
[4]*State Key Laboratory of Surface Physics and Department of Physics, Fudan University, Shanghai 200433, China*
[5]*Shanghai Institute of Applied Physics, CAS, Shanghai, China*

A central key to understanding heavy-fermion systems involves revealing how itinerant low-energy excitations emerge from local f moments. An effective way to understand the f-electron behavior is to compare the electronic structure of f-electron compounds with a reference isostructural compound with no f electrons. Here we present a systematic electronic structure study of $LaCoIn_5$, which is a non-f reference compound of the heavy-fermion superconductor $CeCoIn_5$. Our angle-resolved photoemission spectroscopy study of the three dimensional Fermi surface and band structure of $LaCoIn_5$ highlights rather three-dimensional electronic character of this compound. The conduction bands of $LaCoIn_5$ are almost identical to that of $CeCoIn_5$, though obvious differences can be found in the low-energy electronic structure. Finally, we give a quantitative analysis of the Fermi pocket change in $LaCoIn_5$ and $CeCoIn_5$, which may be helpful for understanding the important 'large' and 'small' Fermi surface issue in heavy-fermion compounds.

PACS numbers: 71.20.Be, 71.15.Mb, 72.15.Gd, 79.60.Bm

INTRODUCTION

The discovery of superconductivity in heavy-fermion compounds containing partially filled shell of f orbitals has stimulated intensive research. The strong correlation of f electrons in these materials gives rise to intriguing physical properties such as quantum criticality, unconventional superconductivity, valence fluctuation and non-Fermi liquid behavior [1–3]. These various unusual properties arise from the subtle interplay between the f electrons and conduction electrons, which is a central challenge in condensed matter physics. Key to understanding heavy-fermion systems is to reveal how the itinerant low-energy excitations emerge from the local f moments. At high temperature, the f electrons are free moments and the Fermi surface contains only bands of conduction electrons, which is normally called a 'small' Fermi surface. At low temperature, the Kondo entanglement of f electrons with conduction electrons leads to the formation of composite heavy quasiparticles, giving rise to a 'large' Fermi surface with f-electron contribution [4–7]. Although the change from 'large' to 'small' Fermi surface upon weakening the f hybridization has been observed by several groups [8–11], quantitative determination of this size change is still challenging, due to the small-energy scales in these systems.

Among the cerium-based heavy-fermion compounds, the layered-structure heavy-fermion superconductor $CeCoIn_5$ has been the focus of intense research due to its unusual properties such as field-induced quantum criticality, unconventional superconductivity, and potentially exotic pairing states such as the Fulde-Ferrell-Larkin-Ovchinikov state [12]. De Haas-van Alphen (dHvA) [13, 14], optical conductivity [15, 16], angle-resolved photoemission spectroscopy (ARPES) [8, 11, 17] and scanning tunneling microscopy (STM) [18–20] measurements, along with theoretical calculations [21], all suggest the presence of the itinerant f electrons in this compound. To understand better its physical properties and low-energy excitation electronic structure, it is helpful to compare with its reference compound $LaCoIn_5$, which has the same crystal structure as $CeCoIn_5$ but with no f electrons. Whereas there has been extensive research on $CeCoIn_5$, there are only a few cases in which $LaCoIn_5$ has been studied. The Fermi surface of $LaCoIn_5$ has been examined by dHvA measurements, and it is proposed that its Fermi surface exhibits some portions that are two dimensional and some that are three dimensional [22]. Raman scattering spectra have been reported for both $CeCoIn_5$ and $LaCoIn_5$, and a comparison has been made [23]. ARPES is a powerful tool to study the Fermi surface and electronic structure of solid materials. By comparing low-energy electronic structure and topology, along with the relative sizes of the Fermi surfaces between $LaCoIn_5$ and $CeCoIn_5$, one can clarify and better understand the f-electron behavior in $CeCoIn_5$. To date, ARPES study on $LaCoIn_5$ has been still lacking.

In the present study, we provide a systematic electronic structure study of $LaCoIn_5$. Three dimensional Fermi surface and band structure are revealed and suggest rather three-dimensional character of this compound, although its crystal structure is two dimensional. The conduction bands of $LaCoIn_5$ are almost identical to that of $CeCoIn_5$, though obvious difference can be found for the low-energy excitations. We also give a quantitative analysis of the Fermi pocket change in $LaCoIn_5$ and $CeCoIn_5$, which shows that the electron-like band enlarges in $CeCoIn_5$, while the hole-like band shrinks. Our results may be helpful for understanding the important 'large' and 'small' Fermi surface issue in heavy-fermion compounds.

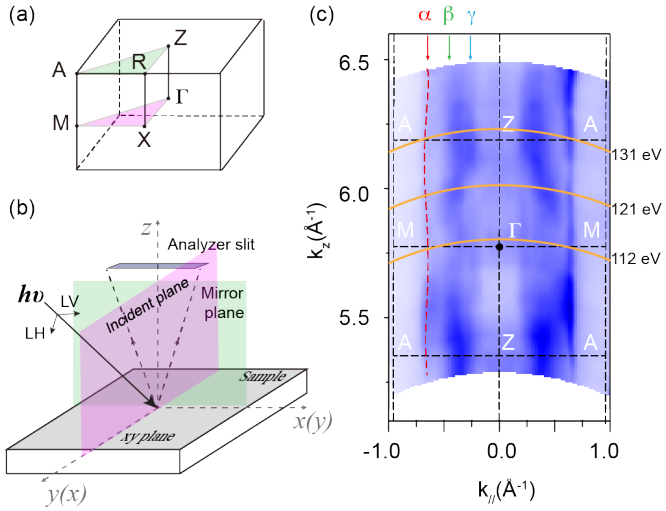

FIG. 1: (a) Brillouin zone of $LaCoIn_5$. (b) Experimental setup for ARPES measurements. (c) Photoemission intensity maps in the Γ*ZAM* plane. The momentum cuts taken with 112, 121 and 131 eV photons in the present study have been marked with the orange solid lines.

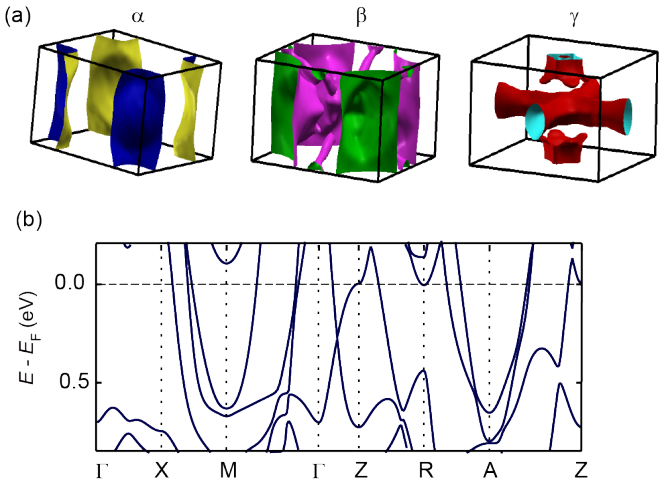

FIG. 2: (a) Calculated three dimensional Fermi surfaces of $LaCoIn_5$. (b) Calculated band structure of $LaCoIn_5$ along the high-symmetry directions.

EXPERIMENTAL AND COMPUTATIONAL DETAILS

Single crystals of $LaCoIn_5$ were grown by the indium self-flux method. Room-temperature x-ray diffraction measurements reveal that all the crystals are single-phase and crystallize in the tetragonal $HoCoGa_5$ structure. The samples were cleaved along the *c*-axis before performing ARPES measurements. Data in Figs. 1-4 were performed at the electron microscopy (ESM) 21-ID-1 beamline of the National Synchrotron Light Source II (NSLS II) equipped with a Scienta DA30 electron analyser, with a base chamber pressure below 1×10^{-11} mbar and temperature of 11 K. Data of $LaCoIn_5$ and $CeCoIn_5$ in Figs. 5 and 6 were obtained at the "Dream-line" beamline at the Shanghai Synchrotron Radiation Facility (SSRF) at 17 K with a Scienta DA30 analyzer; the vacuum was kept below 2×10^{-10} mbar. The overall energy resolution is better than 20 meV, and the angular resolution is 0.1°.

The electronic structure calculations for bulk $LaCoIn_5$ within the density functional theory (DFT) framework were performed with a plane-wave basis projected augmented wave method, as implemented in the Vienna Ab-initio Software Package (VASP) [24]. The spin-orbit coupling effect is considered using a second variational step. The Perdew-Burke-Ernzerhof (PBE) flavor [25] of the generalized gradient approximation is adopted to describe the exchange-correlation of the valence electrons. In all calculations, the experimental lattice constants of $LaCoIn_5$ from Ref. [26] are adopted. An energy cutoff of 400 eV and $21 \times 21 \times 13$ *k*-mesh in the Monkhorst-Pack scheme [27] are employed to converge the static self-consistent calculation to better than 1 meV/atom. Based on the charge density obtained from static calculation, the three-dimensional band structure and Fermi surfaces are obtained. The *k*-meshs for two dimensional and three dimension Fermi surface calculation are $60\times60\times1$ and $22\times22\times14$, respectively.

RESULTS AND DISCUSSIONS

Figure 1(a) presents the three dimensional Brillouin zone of $LaCoIn_5$ with all the high symmetry plane and high symmetry points indicated. The experimental setup for our ARPES measurements is shown in Fig. 1(b). During ARPES measurements, both linear vertical (LV) and linear horizontal (LH) polarized photons are used, in that case bands with different orbitals will be pronounced in different polarizations. For standard ARPES measurements, the in-plane momentum $k_{\|}$ can be determined by the momentum conservation of photoelectrons [28], while the determination of the out-of-plane momentum component (k_z) is less straightforward. However, it can still be indirectly obtained by performing a set of ARPES measurements under different photon energies [29, 30]. Based on the nearly free-electron final state approximation with the inner potential parameter V_0 (describing the energy difference from the bottom of the final state band to the vacuum level), we can derive k_z as [29–31]: $k_z = (1/\hbar)\sqrt{2m(E_{kin}\cos^2\theta + V_0)}$, where θ is the emission angle of the photoelectron relative to the surface normal, m is the effective mass of electrons in the final bulk states and E_{kin} is the kinetic energy of the emitted electrons [31]. To determine V_0 of $LaCoIn_5$, we performed three dimensional Fermi surface mapping using a broad range of photon energies (from 90 eV to 144 eV), which covers a sufficient range of more than one Brillouin zone along the k_z direction.The photon energies used here nicely illustrate the three dimensional band evolutions, indicating the ability to detect the bulk states. Based on the three dimensional Fermi surface map in Fig. 1(c), the inner potential value for $LaCoIn_5$ here is 21 eV, to match the periodiocity of the bands.

From Fig. 1(c), three different bands can be resolved con-

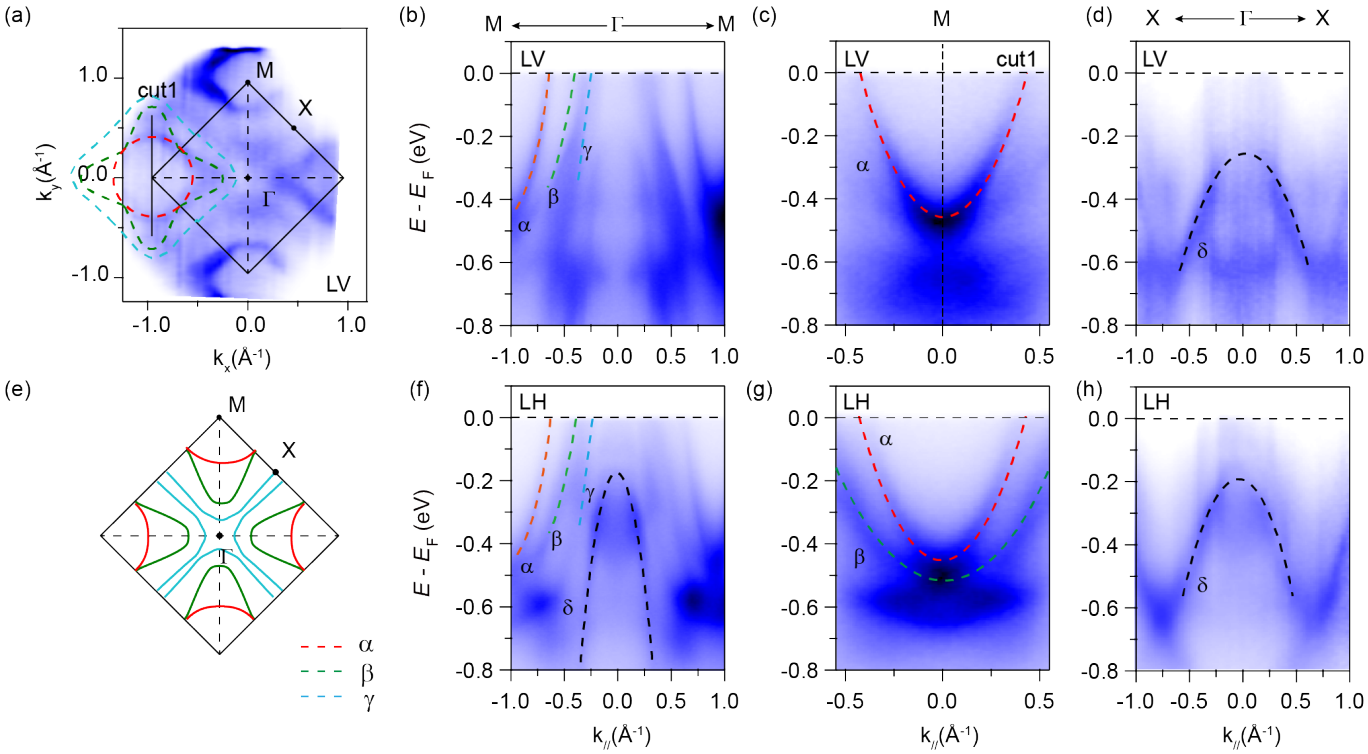

FIG. 3: (a) Photoemission intensity map of $LaCoIn_5$ in the ΓXM plane taken with 112 eV LV-polarized photons. (b-d) Photoemission intensity distributions along the ΓM direction (b), (c) cut1 in (a), ΓX direction (d) with LV-polarized light. (e) Schematic Fermi surface sheet of the ΓXM plane by tracking Fermi crossings of panel (a). (f-h) Photoemission intensity distributions along the ΓM direction (f), (g) cut1 in (a), ΓX direction (h) with LH-polarized light.

tributing to the Fermi surface of $LaCoIn_5$, named α, β and γ, respectively. Among them, the dispersion of the α band can be clearly traced, which is a corrugated cylindrical sheet along the k_z direction with rather two-dimensional character. For the β and γ Fermi surfaces, the dispersions are hard to trace, indicating a rather three dimensional nature of these two bands. Our experimental results are consistent with theoretical calculations, as shown in Fig. 2(a). From Fig. 2(a), the topologies of the three Fermi surfaces can be clearly observed. Among them, the α Fermi surface is the most two dimensional with corrugated cylindrical sheets having a maximum and minimum. For the β Fermi surface, although part of the Fermi surface is also cylindrical, it is more corrugated than the α Fermi surface, showing rather three dimensional character. For the γ Fermi surface, it has been separated into two parts with a small pocket in the ZAR plane and a large cross-shaped pocket in the ΓXM plane.

Figure 3(a) displays the photoemission intensity map in the ΓXM plane taken with 112 eV LV-polarized photons. The Fermi surface for the ΓXM plane is composed of three pockets: a rounded α pocket, a flower-shaped β pocket, and a large square-like γ pocket. Fig. 3(e) summarizes the schematic Fermi surface sheet of the ΓXM plane by tracking Fermi crossings in Fig. 3(a), which qualiatively agrees well with theoretical calculations. Figs. 3(b-d) show the photoemission intensity plots along several high-symmetry directions with LV polarization. From Fig. 2(b), it is clear that three bands, named α, β and γ, cross the Fermi level, which contributes the three pockets in Fig. 1(a). The α band is parabolic like, with its bottom located at 0.48 eV binding energy. For the ΓX direction, we did not observe an obvious band crossing the Fermi level. Photoemission intensity plots taken with LH polarization are shown in Figs. 3(f-h), and the three bands can all be observed with LH polarization. Additionally, a δ band locating at much higher binding energy can be observed.

Figure 4(a) displays the photoemission intensity map in the ZAR plane taken with 131 eV LV-polarized photons. In the ZAR plane, the flower-shaped β pocket in the ΓXM plane turns out to be rounded in the ZAR plane, while the rounded α pocket turns out to be square-like. A dramatic change can be found for the γ pocket, in the ZAR plane it shrinks to a small square-like pocket around the Brillouin zone center. One might notice that due to the effect of k_z broadening [33], some features in the ΓXM plane can also be found in the ZAR plane, although much weaker. For example, the flower-shaped β pocket also has some finite intensity in the ZAR plane. Figs. 4(b-d) and 4(f-h) show the band structure along several high-symmetry directions with LV and LH polarized light, respectively. The dispersion of the three bands can be more clearly observed in the ZAR plane. There are three main features that are different from what is observed in the ΓXM plane: 1) the γ band can be observed crossing the Fermi level in Fig.

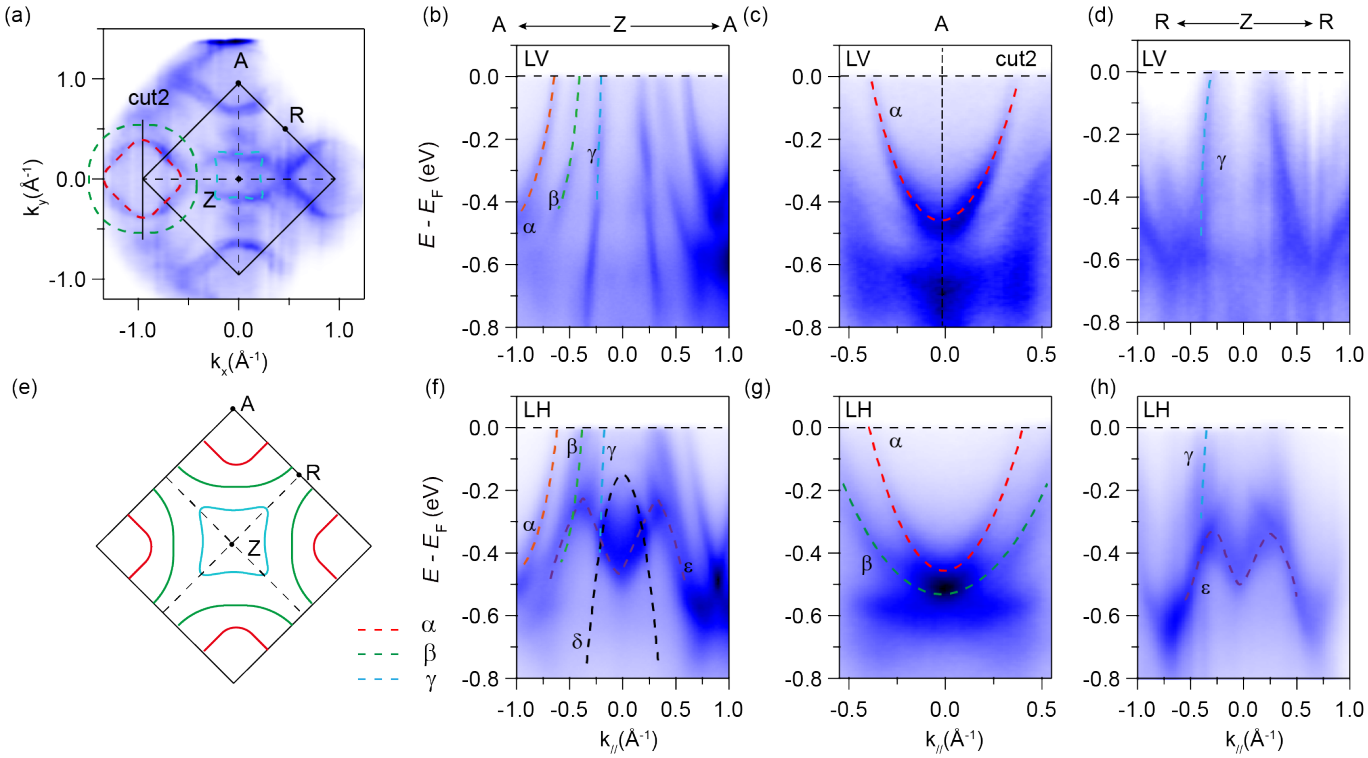

FIG. 4: (a) Photoemission intensity map of $LaCoIn_5$ in the ZAR plane taken with 131 eV LV-polarized photons. (b-d) Photoemission intensity distributions along the ZA direction (b), (c) cut2 in (a), ZR direction (d) with LV-polarized light. (e) Schematic Fermi surface sheet of the ZAR plane by tracking Fermi crossings of panel (a). (f-h) Photoemission intensity distributions along the ZA direction (f), (g) cut2 in (a), ZR direction (h) with LH-polarized light.

4(d), which contributes the small square-like pocket around the zone center. 2) The size of the α pocket shrinks in the ZAR plane. This is in agreement with photoemission intensity map along the k_z direction in Fig. 1(c). From Fig. 1(c), the α pocket has a maximum cross section in the ΓXM plane and a minimum cross section in the ZAR plane. 3) an 'M'-shaped ε band can be found with LH polarization in Fig. 4(f).

Although the crystal structure of $LaCoIn_5$ is layered, from our results the Fermi surface of $LaCoIn_5$ is not two dimensional. The α Fermi surface is the most two dimensional one with corrugated cylindrical sheets, while both the β and γ Fermi surfaces are three dimensional with the γ Fermi surface being the most three dimensional one. Our ARPES results of the shapes of the α and β pockets agree qualitatively with previous dHvA measurements [14], which also observed the corrugated cylindrical α sheet and a highly-corrugated β sheet. Our results provide more information about the γ Fermi surface: the dHvA measurements do not provide the shape and k_z dependence of the γ pocket due to the low frequency of this branch.

The heavy fermion behaviour of strongly correlated $4f$-electron compounds has attracted tremendous interest in the condensed matter physics field. Central to understanding heavy-fermion systems is the interplay between the f electrons and conduction electrons. To better understand the electronic structure of $CeCoIn_5$, especially the low-energy excitations, it is helpful to compare the electronic structure of $CeCoIn_5$ and $LaCoIn_5$, which is a non-$4f$ analog of $CeCoIn_5$. Fig. 5 shows the comparison of the electronic structure between $CeCoIn_5$ and $LaCoIn_5$ taken with 121 eV photons, which is the resonant condition for $CeCoIn_5$ at the Ce $4d$-$4f$ transition to enhance the f-electron photoemission intensity. The band structure of $LaCoIn_5$ away from the Fermi level is almost identical to that of $CeCoIn_5$, as is also found in Ref. [8], exhibiting obvious dispersions. The main difference between the two compounds is in the low-energy electronic structure. In $CeCoIn_5$, a nearly flat band displaying a weak dispersion around the Γ point can be found in the vicinity of the Fermi level in Fig. 5(d), which is absent in $LaCoIn_5$. This further demonstrates that the nearly flat band near the Fermi level is intrinsic and mainly from the f electrons. Figs. 5(a) and 5(b) show the Fermi surface mapping of $LaCoIn_5$ and $CeCoIn_5$, respectively. The obvious difference between the two compounds is that there is large intensity of spectral weight around the Brillouin center, which originates from the f states near the Fermi level. Fig. 5(e) shows the angle-integrated energy distribution curves (EDCs) for $LaCoIn_5$ and $CeCoIn_5$. Two nearly flat bands can be observed in $CeCoIn_5$: the one near the Fermi level is the tail of the Kondo resonance, which can be attributed to the $4f^1_{5/2}$ state, while another one located at 0.27 eV binding energy is its spin-orbit-split $4f^1_{7/2}$

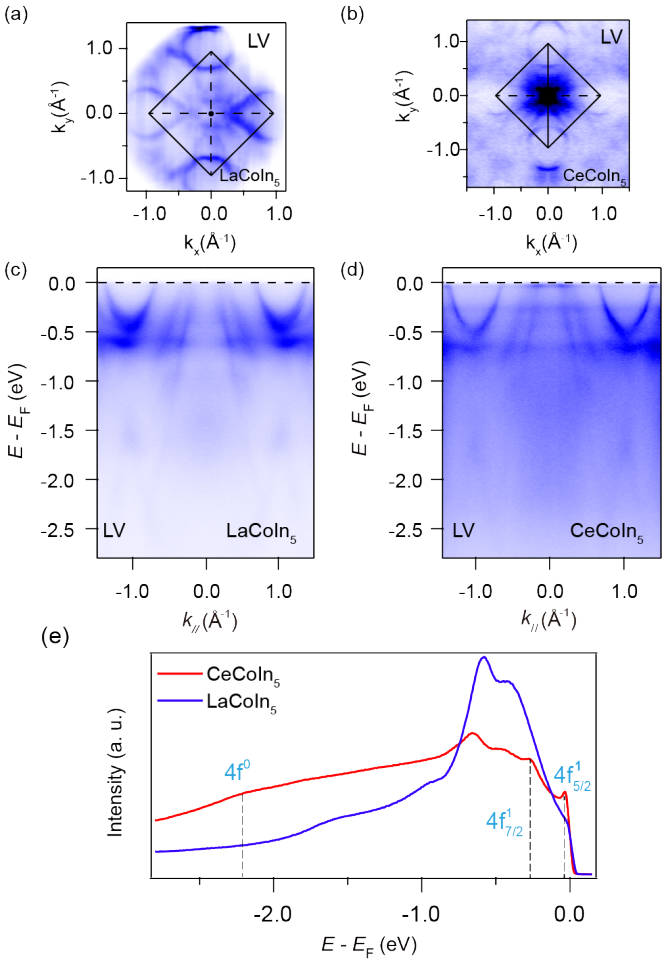

FIG. 5: (a) Photoemission intensity map of $LaCoIn_5$ taken with 121 eV LV-polarized photons. (b) Photoemission intensity map of $CeCoIn_5$ taken with 121 eV LV-polarized photons, which has been reported in our previous study [8]. We plot it here again to give a direct impression of the Fermi surface change in the two compounds. (c) Photoemission intensity distributions of $LaCoIn_5$ taken along the Γ-M direction with LV-polarized light. (d) Photoemission intensity distributions of $CeCoIn_5$ taken along the Γ-M direction with LV-polarized light. The low-energy band structure can also be found in Ref. [8]. (e) Angle-integrated EDCs for data in panels (a) and (b) for $LaCoIn_5$ and $CeCoIn_5$. The f-band peak positions for $CeCoIn_5$ are highlighted.

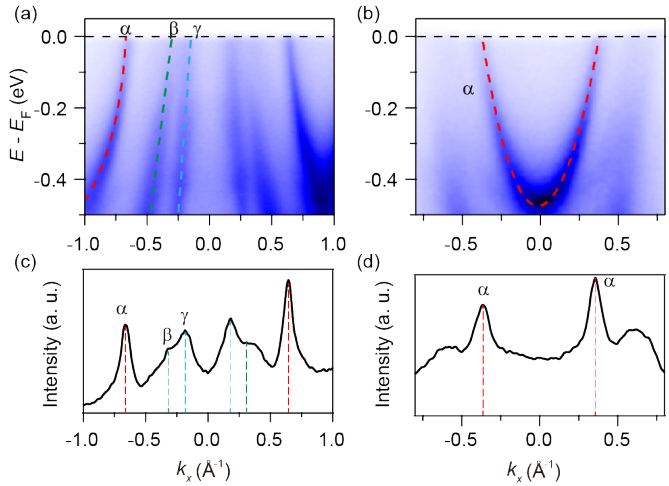

FIG. 6: (a) Zoom-in of the photoemission intensity distribution of $LaCoIn_5$ in Fig. 5(a). (b) Zoom-in of the photoemission intensity distribution for the α pocket of $LaCoIn_5$. (c) Corresponding MDC at the Fermi level of panel (a). (d) Corresponding MDC at the Fermi level of panel (b).

component. In its sister compounds $CeIrIn_5$ and $CeRhIn_5$, besides the $4f^1_{5/2}$ and $4f^1_{7/2}$ components, the $4f^0$ state can also be observed, located at around 2.3 eV [31, 34]. While in $CeCoIn_5$, we do not observe an obvious flat band at higher binding energy. From Fig. 5(c), only a small hump located at 2.2 eV can be found, which mainly comes from the the $4f^0$ state.

In heavy-fermion systems, at high temperature, the f electrons behave as local moments, which do not 'talk' with the conduction electrons, and the Fermi surface is normally called a 'small' Fermi surface. As the temperature is lowered, the entanglement between the f electrons and conduction electrons leads to the formation of heavy quasiparticles [9]. At this stage, the f electrons participate in the formation of the Fermi surface, resulting in a 'large' Fermi surface with f-electron contribution. In our previous study of $CeCoIn_5$, we have given a quantitative analysis of the Fermi surface change between 145 K and 17 K, estimating that the radius of the α electron pocket expands by 0.024 ± 0.008Å^{-1} between 145 K and 17 K, while the radius of the γ hole pocket shrinks by 0.042 ± 0.008Å^{-1} in this temperature range. By comparing the electronic structure of $CeCoIn_5$ and $LaCoIn_5$, especially the Fermi crossings of different bands, we can give a more direct quantitative evaluation of the Fermi pocket change due to the inclusion of f electrons. Figure 6(a) shows a zoom-in of the ARPES data of Fig. 5(c), and its corresponding momentum distribution curves (MDCs) are displayed in Fig. 6(c). From Fig. 6(c), the Fermi energy crossings for the α, β and γ bands are found to be 0.65, 0.31, 0.16 Å^{-1} in $LaCoIn_5$, respectively. To directly compare the size of the α pocket in $CeCoIn_5$ and $LaCoIn_5$, Figs. 6(b) and 6(d) show the ARPES data for the left α pocket and its corresponding MDC, from which the radius for the α pocket is found to be 0.350 Å^{-1}. In $CeCoIn_5$, the Fermi momentum for the γ band is found to be 0.9 Å^{-1} at 17 K, compared to that of 0.132 Å^{-1} at 145 K. For the α pocket, its radius is 0.37 Å^{-1}, while is 0.346 Å^{-1} at 145 K. Based on the quantitative analysis, we estimate that the radius of the α electron pocket expands by 0.02 ± 0.008Å^{-1} between $LaCoIn_5$ and $CeCoIn_5$ at 17 K. The radius of the α pocket in $LaCoIn_5$ is almost the same as that of $CeCoIn_5$ at 145 K, indicating that the entanglement between the f electrons and this conduction band is almost absent at this temperature. While for the γ band, the radius of this hole pocket shrinks by 0.07 ± 0.008Å^{-1} in $LaCoIn_5$ and $CeCoIn_5$ at 17 K. It is noteworthy that, by comparing with the Fermi momen-

tum for the γ band in $LaCoIn_5$, we find that the γ band in $CeCoIn_5$ at 145 K also shinks $0.028 \pm 0.008 Å^{-1}$, indicating that the entanglement between the conduction electrons and f electrons may already start at 145 K in $CeCoIn_5$. Due to the overlap of several bands after hybridization in $CeCoIn_5$, it is hard to observe the exact Fermi momentum of the β band, thus we can not compare the change for this band in the two compounds. From our results, we find that the most two dimensional α band in $CeCoIn_5$ shows the weakest hybridization with f states, while the more three dimensional γ band shows stronger hybridization. Moreover, a size change of the γ band between $LaCoIn_5$ and $CeCoIn_5$ at 145 K is found, which indicates that Kondo entanglement between the f electrons and conduction electrons already starts at this temperature, much higher than the coherent temperature of 50 K for $CeCoIn_5$. This is consistent with our previous results of $CeCoIn_5$ [8].

CONCLUSION

In summary, we present a comprehensive electronic structure study of the non f-electron compound $LaCoIn_5$, which is a reference compound for the important heavy-fermion superconductor $CeCoIn_5$. Our results find that although its crystal structure is two-dimensional, the electronic structure shows rather three-dimensional character. By comparing the electronic structure, especially the low-energy excitations of $LaCoIn_5$ and $CeCoIn_5$, the contributions of f electrons in $CeCoIn_5$ can be clearly identified. Moreover, we find that the electron-like band enlarges in $CeCoIn_5$, while the hole-like band shrinks. We further give a quantitative analysis of the change of these bands in $LaCoIn_5$ and $CeCoIn_5$, which provides an important clue for understanding the 'large' and 'small' Fermi surface issue in these materials.

ACKNOWLEDGMENTS

This work is supported by the Science Challenge Project (Grants No. TZ2016004), the National Science Foundation of China (Grants No. 11874330, U1630248), the National Key Research and Development Program of China (No. 2017YFA0303104) and the U.S. Department of Energy, Office of Science, Office of Basic Energy Sciences under Award Number DE-SC0019211. Operation of ESM beamline at the National Synchrotron Light Source is supported by U.S. Department of Energy (DOE) Office of Science User Facility Program operated for the DOE Office of Science by Brookhaven National Laboratory under Contract No. DE-AC02-98CH10886.

* Electronic address: chenqiuyun@caep.cn
† Electronic address: juan.jiang@yale.edu

[1] P. Coleman, and Anddriy H. Nevidomskyy, Frustration and the Kondo effect in heavy fermion materials, J. Low. Temp. Phys. **161**, 182 (2010).
[2] C. M. Varma, Mixed-valence compounds, Rev. Mod. Phys. **48**, 219 (1976).
[3] G. R. Stewart, Heavy-fermion systems, Rev. Mod. Phys. **56**, 755 (1984).
[4] S. Nakatsuji, S. Yeo, L. Balicas, Z. Fisk, P. Schlottmann, P. G. Pagliuso, N. O. Moreno, J. L. Sarrao, and J. D. Thompson, Intersite coupling effects in a Kondo lattice, Phys. Rev. Lett. **89**, 106402 (2002).
[5] B. Cornut and B. Coqblin, Influence of the crystalline field on the Kondo effect of alloys and ccompounds with cerium impurities, Phys. Rev. B **5**, 4541 (1972).
[6] T. Pruschke, R. Bulla, and M. Jarrell, Low-energy scale of the periodic Anderson model, Phys. Rev. B **61**, 12799 (2000).
[7] S. Burdin, A. Georges, and D. R. Grempel, Coherence scale of the Kondo lattice, Phys. Rev. Lett. **85**, 1048 (2000).
[8] Q. Y. Chen, D. F. Xu, X. H. Niu, J. Jiang, R. Peng, H. C. Xu, C. H. P. Wen, Z. F. Ding, K. Huang, L. Shu. Y. J. Zhang, H. Lee, V. N. Strocov, M. Shi, F. Bisti, T. Schmitt, Y. B. Huang, P. Dudin, X. C. Lai, S. Kirchner, H. Q. Yuan, and D. L. Feng, Direct observation of how the heavy-fermion state develops in $CeCoIn_5$, Phys. Rev. B **96**, 045107 (2017).
[9] J. H. Shim, K. Haule, and G. Kotliar, Modeling the localized-to-itinerant electronic transition in heavy fermion system $CeIrIn_5$, Science **7318**, 1615 (2007).
[10] H. C. Choi, B. I. Min, J. H. Shim, K. Haule, and G. Kotliar, Temperature-dependent Fermi surface evolution in heavy fermion $CeIrIn_5$, Phys. Rev. Lett. **108**, 016402 (2012).
[11] Sooyoung Jang, J. D. Denlinger, J. W. Allen, V. S. Zapf, M. B. Maple, Jae Nyeong Kim, Bo Gyu Jang, and Ji Hoon Shim, Evolution of the Kondo lattice electronic structure above the transport coherence temperature, arXiv:1704.08247.
[12] B.-L. Young, R. R. Urbano, N. J. Curro, J. D. Thompson, J. L. Sarrao, A. B. Vorontsov, and M. J. Graf, Microscopic Evidence for Field-Induced Magnetism in $CeCoIn_5$, Phys. Rev. Lett. **98**, 036402 (2007).
[13] R. Settai, H. Shishido, S. Ikeda, Y. Murakawa, M. Nakashima, D. Aoki, Y. Haga, H. Harima, and Y. Ōnuki, Quasi-two-dimensional Fermi surfaces and the de Haas-van Alphen oscillation in both the normal and superconducting mixed states of $CeCoIn_5$, J. Phys.:Condens. Matter **13**, L627 (2001).
[14] H. Shishido, R. Settai, D. Aoki, S. Ikeda, N. Nakamura, T. Iizuka, Y. Inada, K. Sugiyama, T. Takeuchi, K. Kindo, T. C. Kobayashi, Y. Haga, H. Harima, Y. Aoki, T. Namiki, H. Sato, and Y.Ōnuki, Fermi Surface, Magnetic and Superconducting Properties of $LaRhIn_5$ and $CeTIn_5$ (T: Co, Rh and Ir), J. Phys. Soc. Jpn. **71**, 162-173 (2002).
[15] E. J. Singley, D. N. Basov, E. D. Bauer, and M. B. Maple, Optical conductivity of the heavy fermion superconductor $CeCoIn_5$, Phys. Rev. B **65**, 161101(R) (2002).
[16] K. S. Burch, S. V. Dordevic, F. P. Mena, A. B. Kuzmenko, D. van der Marel, Optical signatures of momentum-dependent hybridization of the local moments and conduction electrons in Kondo lattices, Phys. Rev. B **75**, 054523 (2007).
[17] A. Koitzsch, T. K. Kim, M. Knupfer, B. Büchner, M. Richter, I. Opahle, R. Follath, E. D. Bauer, and J. L. Sarrao, Band-dependent emergence of heavy quasiparticles in $CeCoIn_5$, Phys. Rev. B **88**, 035124 (2013).
[18] P. Aynajian, E. H. da Silva Neto, A. Gyenis, R. E. Baumbach, J. D. Thompson, Z. Fisk, E. D. Bauer, and A. Yazdani, Visualizing

heavy fermions emerging in a quantum critical Kondo lattice, Nature **486**, 201 (2012).

[19] M. P. Allan, F. Massee, D. K. Morr, J. Van Dyke, A. W. Rost, A. P. Mackenzie, C. Petrovic, and J. C. Davis, Imaging Cooper pairing of heavy fermions in $CeCoIn_5$, Nat. Phys. **9**, 468 (2013).

[20] B. B. Zhou, S. Misra, E. H. da Silva Neto, P. Aynajian, R. E. Baumbach, J. D. Thompson, E. D. Bauer, and A. Yazdani, Visualizing nodal heavy fermion superconductivity in $CeCoIn_5$, Nat. Phys. **9**, 474 (2013).

[21] K. Haule, C-H. Yee, and K. Kim, Dynamical mean-field theory within the full-potential methods: Electronic structure of $CeIrIn_5$, $CeCoIn_5$, and $CeRhIn_5$, Phys. Rev. B **81**, 195107 (2010).

[22] D. Hall, and L. Balicas, High-field de Haas van Alphen studies of the Fermi surfaces of $LaMIn_5$ (M=Co,Rh, Ir), Phys. Rev. B **79**, 033106 (2009).

[23] H. Martinho, P. G. Pagliuso, V. Fritsch, N. O. Moreno, J. L. Sarrao, and C. Rettori, Vibrational and electronic excitations in the (Ce, La)MIn$_5$(M=Co,Rh) heavy-fermion family, Phys. Rev. B **75**, 045108 (2007).

[24] G. Kresse, J. Hafner, Ab initio molecular dynamics for liquid metals, Phys. Rev. B **47**, 558-561(1993).

[25] J. P. Perdew, K.Burke, M. Ernzerhof, Generalized Gradient Approximation Made Simple, Phys. Rev. B **77**, 3865-3868(1996).

[26] R. T. Macaluso, J. L. Sarrao, P. G. Pagliuso, N. O. Moreno, R. G. Goodrich, D. A. Browne, F. R. Fronczek, and J. Y. Chan, Crystal Growth and Structure Determination of $LaMIn_5$ (M=Co, Rh, Ir), J. Solid State Chem. **245**, 166(2002).

[27] J. Monkhorst and J. D. Pack, Special points for Brillouin-zone integrations, Phys. Rev. B **13**, 5188(1976).

[28] Y. Chen, Studies on the electronic structures of three-dimensional topological insulators by angle resolved photoemission spectroscopy, Front. Phys. **7**, 175-192 (2012).

[29] A. Damascelli, Probing the electronic structure of complex systems by ARPES,Physica Scripta **T109**, 61-74 (2004).

[30] A. Damascelli, Z. Hussain, and Z.-X. Shen, Angle-resolved photoemission studies of the cuprate superconductorsAngle-resolved photoemission studies of the cuprate superconductors, Rev. Mod. Phys.75, 473-541(2003).

[31] Q. Y. Chen, D. F. Xu, X. H. Niu, R. Peng, H. C. Xu, C. H. P. Wen, X. Liu, L. Shu, S.Y. Tan, X. C. Lai, Y. J. Zhang, H. Lee, V. N. Strocov, F. Bisti, P. Dudin, J.-X. Zhu, H. Q. Yuan, S. Kirchner, and D. L. Feng, Band dependent interlayer f-electron hybridization in $CeRhIn_5$, Phys. Rev. Lett. **120**, 066403(2018).

[32] S.-I. Fujimor, Y. Takeda, T. Okane, Y. Saitoh, A. Fujimor, H. Yamagami, Y. Haga, E. Yamamoto, and Y. Onuki, Electronic structures of uranium compounds studied by soft X-ray photoelectron spectroscopy, J. Phys. Soc. Jpn. **85**, 062001(2016).

[33] K. Horiba, M. Kitamura, K. Yoshimatsu, M. Minohara, E. Sakai, M. Kobayashi, A. Fujimori, and H. Kumigashira, Isotropic kink and quasiparticle excitations in the three-dimensional perovskite manganite $La_{0.6}Sr_{0.4}MnO_3$, Phys. Rev. Lett. **116**, 076401(2016).

[34] Q. Y. Chen, C. H. P. Wen, Q. Yao, K. Huang, Z. F. Ding, L. Shu, X. H. Niu, Y. Zhang, X. C. Lai, Y. B. Huang, G. B. Zhang, S. Kirchner, and D. L. Feng, Tracing crystal-field splittings in the rare-earth-based intermetallic $CeIrIn_5$, Phys. Rev. B **97**, 045149(2018).